공학석사 학위논문

Estimation of Fatigue Life of Additive Manufactured AlSi10Mg by Strain-Life Method and Fracture Mechanical Approach

변형률-수명 방법과 파괴역학 접근에 의한 적층제조된 AlSi10Mg의 피로수명 평가

2021 년 2 월

서울대학교 대학원

항공우주공학과

송 윤 선

Estimation of Fatigue Life of Additive Manufactured AlSi10Mg by Strain-Life Method and Fracture Mechanical Approach

변형률-수명 방법과 파괴역학 접근에 의한
적층제조된 AlSi10Mg의 피로수명 평가

지도 교수 윤 군 진

이 논문을 공학석사 학위논문으로 제출함
2021 년 2 월

서울대학교 대학원
항공우주공학과
송 윤 선

송윤선의 공학석사 학위논문을 인준함
2021 년 2 월

위 원 장 김 지 환 (인)

부위원장 윤 군 진 (인)

위 원 김 도 년 (인)

Abstract

Estimation of Fatigue Life of Additive Manufactured AlSi10Mg by Strain-Life method and Fracture Mechanical Approach

Yunsun Song
Department of Aerospace Engineering
The Graduate School
Seoul National University

The alloy manufactured by the selective laser melting method, which is widely known in 3D printing technology / Additive manufacturing (AM), has advantages in design flexibility and production efficiency compared to the conventional process. Titanium and aluminum (Al) alloys processed by AM are commonly used in aviation and medical fields. However, in this process, heat treatment is performed to remove internal defects such as pores in the alloy, although complete removal is inevitable. For this reason, the fatigue life of AM alloy should be evaluated in consideration of

the effect of pores. In this thesis, the fatigue life was analyzed by generating a representative volume element (RVE) with pores as computed tomography (CT) image of an Al alloy processed by AM. For fatigue life analysis, the strain-life method was applied to the crack initiation cycle and Fracture Mechanical approach was applied to the crack propagation cycle. RVE was generated by increasing the image's quality and separating the pores of the CT image through an image processing algorithm. Stress and strain were obtained through 3D finite element (FE) analysis by applying periodic boundary conditions to multiple RVEs for statistical analysis. The value required for fatigue life analysis and FE analysis was calculated using commercial software ABAQUS, and FE-SAFE and the total fatigue life was calculated through post-processing and numerical integration by Python script and MATLAB code. As a result of analyzing the relationship between the pore information of the RVE and the fatigue life, the volume of pores was a critical factor, and compared with the experimental results of reference. It was good agreement that the fatigue life values of multiple RVEs had a somewhat similar range.

Keywords : Additive manufacturing, Fatigue life, Fracture Mechanics
Crack initiation and propagation, Strain−life approach,
Student Number : 2019−28564

Table of contents

List of figures

List of tables

1. Introduction

1.1. Motivation

Aerospace industries have employed Additive manufacturing (AM) to fabricate aircraft components since AM developed in late 1980 [1, 2]. AM is joining materials to make objects from 3D model data, usually layer upon layer, instead of subtractive manufacturing methodologies [3]. Unlike conventional methods of manufacturing, AM has no intermediate process and can be corrected immediately. Because of the rapid design-to-manufacture cycle and higher costs efficiency, AM is widely applied in aerospace industries and in the automobile and medical fields [4-6].

One of additive manufacturing, the Selective Laser Melting (SLM) process, is commonly used to manufacture aerospace structural parts with Aluminum/Titanium alloys. SLM is defined as a process that the laser is injected into the area to be melt after applying the metal powder as a thin layer and repeat it. SLM is one of the laser powder bed fusion (PBF) and can produce complex shape

products that are difficult to manufacture with conventional methods such as casting and cutting [7]. Unlike materials by other manufacturing processes, the SLM process is affected by laser and material factors such as laser scan speed and power, scan strategy, powder materials, and size [7–10]. These factors affect product modeling and form defects, which influence mechanical properties [11]. Drawbacks of the SLM process are these defects and residual stress. One of these defects is porosity as gas entrapment during insufficient /incomplete melting and rapid solidification. Porosity is a significant cause of low fatigue strength [12, 13], and almost all the fatigue cracks initiate from a pore [8]. So Hot Isostatic Press (HIP) process to remove these pores to enhance fatigue strength. But this HIP process cannot be processed entirely [9, 14]. These defects that cannot be removed influence fatigue life. Therefore, it is vital to know the effect of porosity by the SLM process on fatigue behavior. Many researchers found that density, morphology, size, and location of porosity influence fatigue properties such as fatigue strength [8, 15–16].

In the current studies, the fatigue life until the fracture is

obtained through a fatigue test to know the effect of defect such as porosity, and then cracks generated in the defect are confirmed in detail through X-ray micro-computed tomography (μCT) of the fractured part. Considering these experimental results, various fatigue life predictions method consistent with the test conditions are used.

Fatigue life prediction methods can be divided into the Stress-life method, Strain-life method, and Fracture Mechanical approach [17, 18]. The stress-life method was first presented by Wohler [19] and the standard fatigue life prediction method for almost 100 years. This is also called S-N approach. In this method, stress of a magnitude lower than ultimate strength is continuously added to collect the number of cycles until fracture and data is repeatedly collected. Based on these data, the graph plotted as life N against nominal stress S is called the S-N curve, as shown in Figure. 1. S-N curve has a limit to obtaining the fatigue life of a part of the structure. It is not reflected in material's geometry and defect such as porosity.

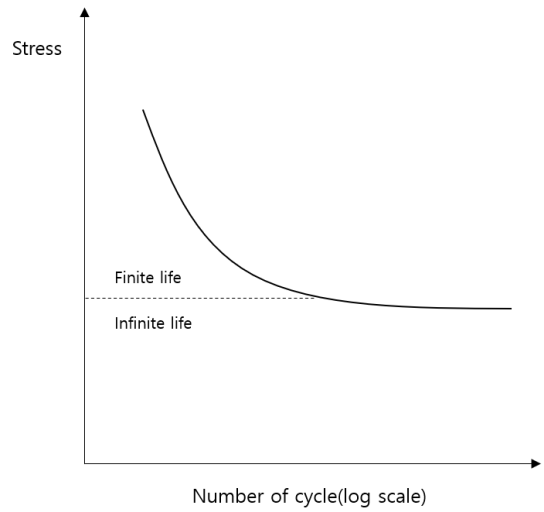

Figure. 1. Schematic S-N curve

The strain-life method is based on the importance that the material's response in critical locations such as notches is strain-dependent in many structures. So, this method is useful for evaluating fatigue life for the local area such as crack, pore, and plastic deformation or strain is measured, while the stress-life method does not. This method is often considered crack initiation life estimates except crack propagation life. This crack propagation life is handled by Fracture Mechanical approach, usually Linear Elastic Fracture Mechanics (LEFM). Fracture Mechanical approach calculates the cycle that crack propagate and fracture using Stress Intensity Factor (SIF) after crack initiation. SIF is the critical factor that depends on

the nominal stress near crack tip and cracks length. Fracture Mechanical approach initially calculated the rate of growth of a crack considering SIF. But gradually considering various conditions such as crack area and stress ratio, several modified models have suggested by Murakami [20], Newman [21], NASGRO [22], etc.

Based on these fatigue life predictions, various modified approaches to the SLM process components are currently being studied. Most of these fatigue life predictions have many models that approach pore size and location[23–25]. Several modified crack propagation model considering SIF calculated $\sqrt{area}$ as a geometrical parameter have been suggested by M. Tang [23] and S. Romano [25]. There are approaches that fatigue life is predicted through pore size distribution measured on a 2D section by scanning electron microscope and modified strain–life parameters based surface roughness [26]. Other approaches such as El HADDAD and TOPPER approach [27] and Danninger–Weiss models [28] consider crack length to estimate fatigue strength for fatigue properties. Siddique et al. [29] use the overall pores developed by CT image influence on stress concentration for fatigue life.

1.2. Objectives and Thesis Overview

In this thesis, we attempt to estimate how porosity affects fatigue life and predict additive manufactured alloys' fatigue life. The total fatigue life is obtained by summing the crack initiation cycle using the strain-life method and propagation cycle through crack growth model based on Fracture Mechanics.

Developing actual CT image of additively manufactured alloy by SLM process to a static finite element (FE) model, there are many elements. So, FE analysis for this model requires a lot of computation time, and we generated several actual representative volume elements (RVE) based on CT image to save time. RVEs generated in MATLAB code were applied cyclic loading, and FE analysis was performed by FE analysis software (ABAQUS 2019). The stress-strain data from ABAQUS simulation was imported to the FE-based fatigue analysis tool (FE-SAFE) to predict crack initiation cycle. FE-SAFE was performed through experimentally determined S-N curve and strain-life method.

After comparing the crack initiation location using FE-SAFE and ABAQUS, the crack was defined, and the crack propagation cycle was

calculated. The post-processed SIF was used to input it into the crack growth model by Python script. The area of the crack until the final fracture occurred was increased to obtain SIF by MATLAB code. After obtaining the SIF until final fracture occurred, the crack propagation cycle was calculated using numerical integration. This crack propagation cycle and crack initiation cycle obtained by FE-SAFE was summed; the total fatigue cycle was obtained. This cycle was verified by comparing it with the experimental results on most similar to the simulation conditions. After calculating the total fatigue cycle of several RVEs through this process, the relationship was confirmed by evaluating the crack initiation position and information of pores.

2. Theoretical background

2.1. Representative volume element approach

Representative volume element (RVE) approach predicts the material's overall behavior by defining a part of the material that is represented as a representative volume factor. Kanit [30] proposed that RVE should be able to accurately predict the overall material behavior through average stress and strain field within the required analysis accuracy. To consider the influence of randomness inside the material, it is possible to deal with the irregularity and randomness inside the material through the process of artificially reconstructing and analyzing a part of the material using a statistical method [31]. Thus, the RVE approach is used to analyze the behavior of various types of heterogeneous microstructures such as composite materials and porous materials [30, 31].

To calculate the effective properties of the RVE model through image processing, a uniform strain must be imposed on the micro-scale RVE. Periodic boundary conditions (PBC), generally are applied to simulate an RVE model. PBC's concept starts with the assumption

that RVE s generated at a random location and the internal structure of the RVE is periodic in the spatial domain. Moreover, kinematic boundary deformation is compatible with those of adjacent RVEs because the internal structures of all surrounding RVEs are identical. PBC can also be applied to the FE model even if it is not a material of the same type of repeated structure [33]. General equation of PBC for RVE is shown as Eq. 1

$$\boldsymbol{u_i = \bar{\varepsilon}_{ik} x_K + u^*_i \ (i,k = 1,2,3)} \quad (1)$$

Where u_i, $\bar{\varepsilon}_{ik}$, x_K, u^*_i are the displacement, the average strain of RVE, the distance between the parallel surfaces, and the item representing periodical component of the displacement on the boundary. Using this equation, we can find the equation for the relative displacement of the three pairs of the opposite boundary surface of RVE (Eq. 2).

$$\boldsymbol{u^{j+}_i - u^{j-}_i = \bar{\varepsilon}_{ik}(x^{j+}_k - x^{j-}_k) = \bar{\varepsilon}_{ik}\Delta x^j_k} \quad (2)$$

Where $j\pm$ means the location(positive, negative) on the boundary surface of RVE, Eq. 2 can be performed through nodal displacement

constraint equations, and the relative displacement vectors ($\vec{U}$) between opposite boundary surfaces of RVE can be calculated (Figure. 2).

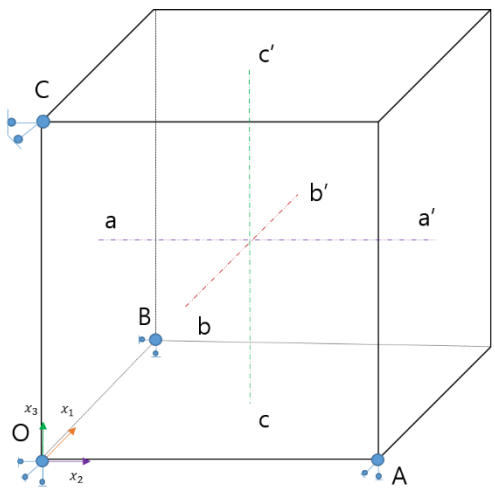

$$\overrightarrow{U_{a'}} = \overrightarrow{U_A} + \overrightarrow{U_a}$$
$$\overrightarrow{U_{b'}} = \overrightarrow{U_B} + \overrightarrow{U_b}$$
$$\overrightarrow{U_{c'}} = \overrightarrow{U_C} + \overrightarrow{U_c}$$

Figure. 2. Schematic of periodic boundary condition

Many studies couldn't show how to apply this PBC to simulate the FE model [34]. To impose PBC on the FE model, boundary node set, displacement boundary conditions, and constraint equations are required. At first, boundary conditions were imposed through direct coding, and it is possible to easily impose PBC by commercial FE software, such as ABAQUS recently.

2.2. Fatigue life prediction

The total fatigue life (N_f) of the structure is primarily divided into two stages: crack formation (N_i) and crack propagation (N_p). The total fatigue life is the sum of crack initiation and cracks propagation [18, 24, 32, 33].

$$N_f = N_i + N_p \tag{3}$$

The fatigue life is sometimes calculated at only one stage, but the total fatigue life is commonly obtained by using an appropriate approach for each of the two stages. In reference [35], the total fatigue life from the crack generation to final failure was well illustrated in block diagram and relevant phase factors were also presented (Figure. 3).

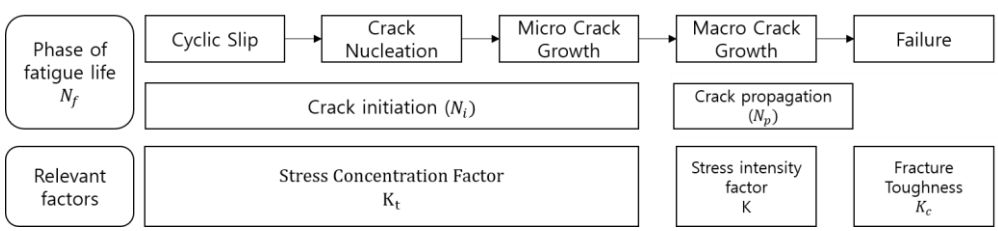

Figure. 3. Phase of the fatigue life and relevant factors

2.2.1. Strain−life method

The crack initiation cycle means fatigue life before the crack is created. The strain−life method is widely used to calculate the crack initiation cycle using the strain−life method's material parameters by the strain−controlled fatigue tests [36]. As Strain−life method, Basquin's equation [37] considering only elastic strain amplitude and Coffin−Manson equation [38], which studied that crack initiation is related to plastic strain, are commonly used. Basquin's equation as

$$\frac{\Delta\sigma}{2} = \frac{\Delta\varepsilon_e}{2} = \frac{\sigma'_f}{E}(2N_f)^b \quad (4)$$

Where ε_e, σ'_f, E, $2N_f$, and b are an elastic component of the cyclic strain amplitude, fatigue strength coefficient, Young's modulus, the number of cycles to failure, and fatigue strength exponent, respectively. Coffin and Manson independently developed an equation considering plastic strain:

$$\frac{\Delta\varepsilon_p}{2} = \varepsilon'_f(2N_f)^c \quad (5)$$

Where ε_p, ε'_f and c are plastic components of strain amplitude, fatigue ductility coefficient, and fatigue ductility exponent. By combining modified Basquin's equation and Coffin−Manson equation can be described total strain amplitude elastic (ε_t) considering the elastic and plastic strain

$$\boldsymbol{\varepsilon_t = \varepsilon_e + \varepsilon_p} \tag{6}$$

$$\boldsymbol{\frac{\Delta\varepsilon_t}{2} = \frac{\sigma'_f}{E}(2N_f)^b + \varepsilon_f'(2N_f)^c} \tag{7}$$

This equation is called the Coffin−Manson equation. However, the Coffin−Manson equation generally does not reflect the mean stress effect (mean stress correction) caused by cyclic loading on the material. The mean stress (σ_m) is the average value of maximum stress (σ_{max}) and minimum stress (σ_{min}) and affects fatigue life (Figure .4).

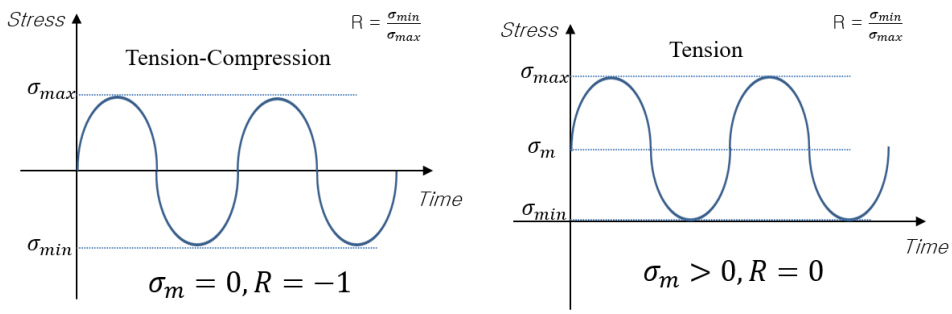

Figure. 4. Stress cycle considering mean stress and load ratio (R)

The effect of mean stress on the Stress amplitude versus the number of cycle curve is shown schematically in Figure. 5, and low load ratio (R) have a longer fatigue life than tests at higher load ratio [39].

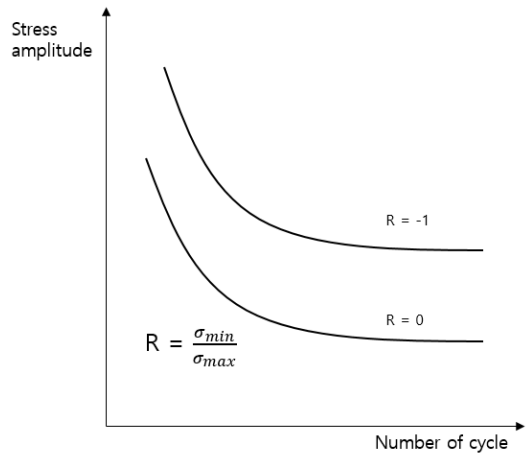

Figure. 5. Effect of mean stress on fatigue life

To account for this effect, Morrow [40] and Smith–Watson–Topper [41] modified the Coffin–Manson equation by including the effect of mean stress. Morrow mean stress correction is given by

$$\frac{\Delta\varepsilon_t}{2} = \frac{\sigma'_f}{E}\left(1 - \frac{\sigma_m}{\sigma'_f}\right)(2N_f)^b + \varepsilon_f'(2N_f)^c \quad (8)$$

Smith–Waston–Topper (SWT) mean stress correction is given by

$$\frac{\Delta\varepsilon}{2}\sigma_{max} = \frac{(\sigma'_f)^2}{E}(2N_f)^{2b} + \sigma'_f\varepsilon_f'(2N_f)^{b+c} \quad (9)$$

Both equations show that mean stress affects longer life, where the elastic strain dominates [41]. The SWT equation predicts no fatigue when the loading is compression and is mainly used when the tensile loading is compared to the Morrow equation. Besides these equations, Brown−miller [42] proposed critical plane analysis with equation as follows

$$\frac{\Delta\gamma_{max}}{2}+\frac{\Delta\varepsilon_n}{2}=1.65\frac{{\sigma_f}^2}{E}\left(2N_f\right)^b+1.75\varepsilon_f{}'\ (2N_f)^c \tag{10}$$

Where $\Delta\gamma_{max}$ is the maximum shear strain and $\Delta\varepsilon_n$ is the normal strain range revolved to the shear stress plane. A multiaxial equation is applied to practical 2D or 3D structures, unlike the equation that only dealt with uniaxial stress or strain.

Additionally, the effect of pores formed by the SLM process is subjected using the stress concentration factor (K_t), which means the ratio of the local maximum elastic stress to the applied stress [42]. K_t is geometric parameter [43] and quantifies how concentrated the stress is in the material part. Through FE analysis using RVE approach, K_t is calculated from the results of ABAQUS.

2.2.2. Fracture Mechanical approach

A study on crack propagation based on Fracture Mechanics has been carried out continuously. The crack growth model was started from well-known Paris's law [44] and numerous fatigue crack growth models considering the effects of various conditions express the crack growth rate (da/dN). A typical fatigue curve is represented using this rate, as shown in Figure. 6.

Paris and Erdogan (1963) proposed Paris's model, which is old and most famous power law that predicts crack growth rate.

$$\frac{da}{dN} = C(\Delta K)^m \quad (11)$$

This equation is calculated the fatigue growth rate with a stress intensity factor and two constants. Stress intensity factor range (ΔK), a standard fracture parameter of numerous crack growth models, is used, and C and m are constants obtained through experiments. K is a parameter representing the elastic stress fields in the vicinity of crack and is expressed as $\Delta K = \Delta\sigma F\sqrt{\pi a}$ where Δσ is the stress range, F is a geometry factor, and a is the crack size.

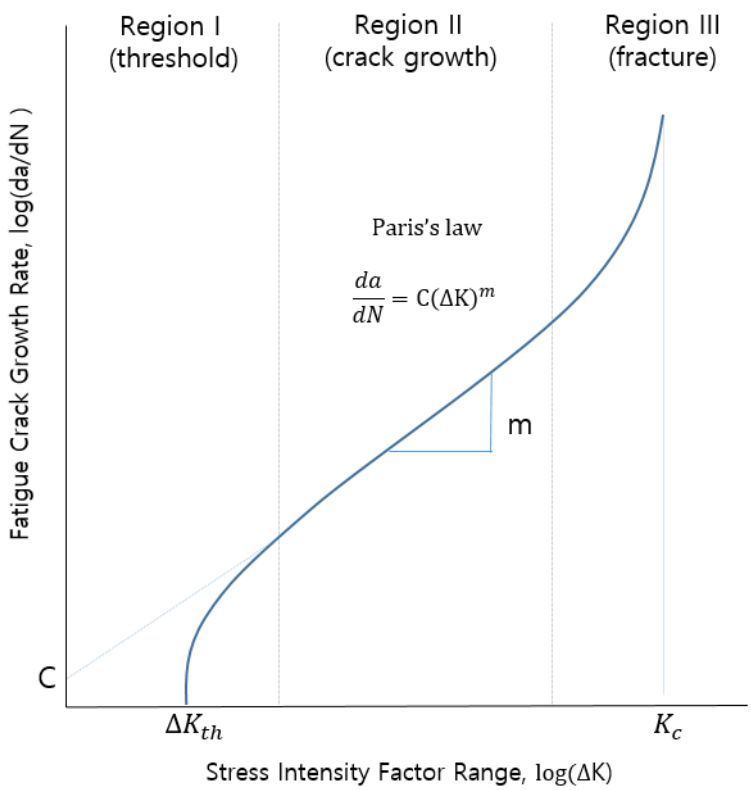

Region I: The threshold value (ΔK_{th}) defined as crack growth threshold

Region II: Stable crack growth accepted linear elastic Fracture Mechanics (LEFM)

Region III: The critical value (K_c) defined as the ability of a material to resist crack growth

Figure. 6. Fatigue curve and relevant factor of regions

K is also related crack driving force, which means the expansion of crack and strain energy release rate [35]. However, Paris's law has limitations in that stress ratio and deals with only data in region II (Figure. 6). Walker model [45] is modified by reflecting the stress ratio (R=K_{min}/K_{max}), which is the limiting point of this Paris model.

$$\frac{da}{dN} = C\left[\frac{\Delta K}{(1-R)^{(1-\lambda)}}\right]^{m} \quad (12)$$

Where C and m are Paris's law constant with R=0, respectively, λ is a material constant. Walker's equation is only valid when R is positive. Walker proposes that when R is negative, the crack is closed and regard it as when R is zero.

Walker model subjects various stress ratio amplitude; it is not described the crack propagation rate in other regions I and II (Figure. 6). Forman (1972) and Nasgro modified model reflected for this problem. Forman model in Eq. 13 is an improved Walker model and is possible to describe the region III until fracture by applying the concept of critical value (K_c). Nasgro model [46] in Eq. 14 can be presented region I (threshold) by using the threshold value (ΔK_{th}).

Constants p, C, m, q are the fitting parameters, which obtained through experiments.

$$\frac{da}{dN} = \frac{C(\Delta K)^m}{(1-R)K_c - \Delta K} \tag{13}$$

$$\frac{da}{dN} = (1 - \frac{\Delta K_{th}}{\Delta K})^p C \left[\frac{1-f}{1-R}\Delta K\right]^m (1 - \frac{\Delta K_{max}}{\Delta K_c})^{-q} \tag{14}$$

In this thesis, the models mentioned above are famous and used in most studies. Other models have been developed to subject the equation with experimental and actual life conditions except for these models. Other models do not use the existing stress intensity factor, such as Murakami's concept with a change in the stress intensity factor, and Dowling and Begley's model using ΔJ instead of ΔK

Murakami' 's concept [47] is an approach using through $\sqrt{area}$ (the square root of the projected area of the defect) and effect of defect size on fatigue life. This method has been widely used for AM materials by SLM process where many defects such as pores occur. Instead of a (crack size) in stress intensity factor, $\sqrt{area}$ is used to predict crack growth rate. K_{max} is maximum value of stress intensity factor determined crack area, expressions are divided according to the crack location.

$$\mathbf{K_{max} = 0.5\sigma\sqrt{\pi\sqrt{area}}}\ \text{(Internal)} \quad (15)$$

$$\mathbf{K_{max} = 0.65\sigma\sqrt{\pi\sqrt{area}}}\ \text{(Surface)} \quad (16)$$

Dowling and Begley model [35] proposes that ΔK was considered a parameter limited only in the elastic phase and invalid in the plastic phase. So, the strain energy release rate, which equals crack driving force for crack growth, is subjected to application in the plastic phase. This strain energy release rate has the same physical meaning as J−integral, which represented fracture energy−based Elastic−Plastic Fracture Mechanics (EPFM), and the equation is shown in Eq. 17.

$$\mathbf{\frac{da}{dN} = C(\Delta J)^m} \quad (17)$$

3. Microstructure modeling including pores

3.1. Material properties

Representative alloys of AM are Titanium and Aluminum alloy, of which CT image of the material for verification by simulation is AlSi10Mg. There are models such as the as-built (AB), stress relief (SR), and HIP process for various purposes. SR as a model that relieves stress by performing heat treatment at low temperature and porosity is not significantly reduced compared to the AB model, but it has been studied in the literature that it affects fatigue resistance [48]. On the other hand, Al alloy treated with the HIP process have pores removed using heat treatment and generally had a longer fatigue life than alloy without heat treatment [49].

In this thesis, as seen in CT image (Figure. 7), fatigue life was studied by extracting RVE for only the AB model with relatively many pores. The porosity calculated by CT scan resulted 0.0061% for As-built. The details of the SLM processing parameters are in Table 1.

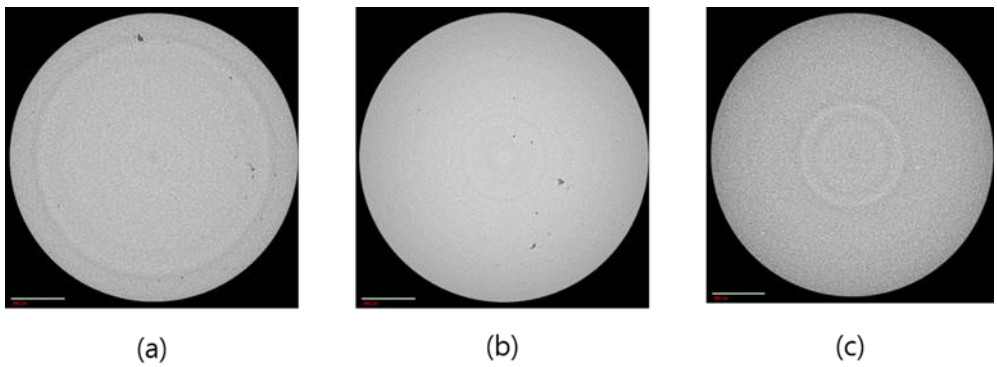

Figure. 7. CT image of SLM AlSi10Mg: (a) As-built, (b) Stress-relief, (c) HIP

Table 1 AM processing parameter for AlSi10Mg

Laser power	370 W
Laser scanning speed	1,300 mm/s
Layer thickness	0.03 mm
Hatch spacing	0.19 mm
Heat treatment	300℃ at 2h (SR)

3.2. Image processing

RVE models were generated using CT images of the As-built (AB) model, and a simulation was performed on them. Using the RVE approach, six RVE models with different pore numbers, sizes, shapes, and locations were randomly selected to evaluate fatigue.

Image processing was performed on the CT image using a MATLAB-based code and a built-in toolbox to generate RVE models. MATLAB's functions were Gaussian filter, median Filter, and erosion to reduce noise in the image. An image with reduced noise was binarized, and particles were separated using a watershed algorithm in MATLAB. Detailed descriptions of filters and algorithms are presented in Table 2. RVE models were composed of a voxel mesh; an input file was created to implement a 3D model of 50x50x50 pixels based on MATLAB code. RVE models with 125,000 elements for FE analysis were developed through the input file, and models are seen in Figure. 8. The pore's information of RVEs such as volume, location, and surface area are in Table 3. Distance to the surface is the distance from the surface to which loading is applied to the center of the pore based on the FE model (0.5mm x 0.5mm x 0.5mm)

Table 2 Image processing description

Image processing algorithm	Description
Gaussian filter	The image is filtered by adding weight to the image with a standard deviation of 0.5, blurring the part with low weight.
Median filter	Filtering using the intermediate value by arranging the surrounding pixels (3−by−3−by−3) in order.
Erosion	Erosion of gray or binarized parts.
Close	Filling the holes in the particles.
Binarized	Matrix area is'0'and a particle area is'1'.
Watershed	Dividing an image from one object into adjacent areas of interest and a bright pixel represents a high, dark pixel at a low elevation and treats it as a curved surface.

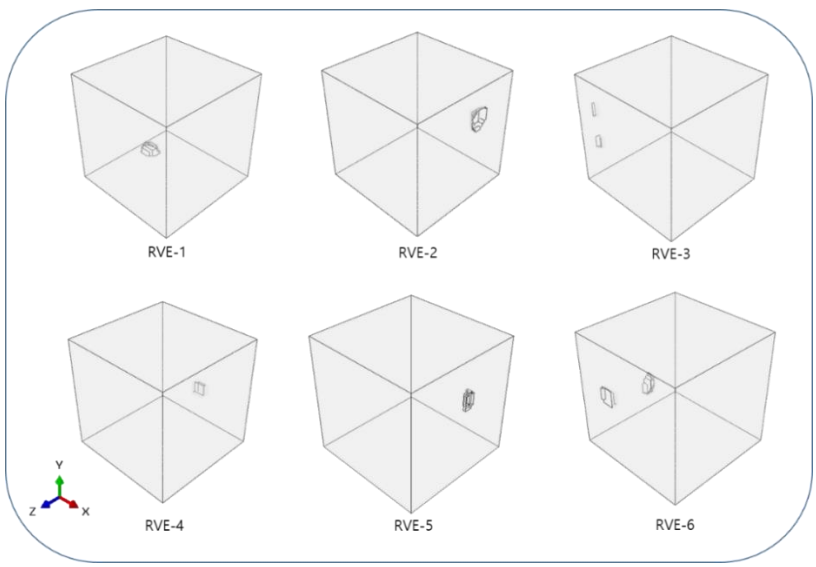

Figure. 8. RVE models generated from CT image

Table 3 Pore information of RVEs

RVE	Pore				
	Shape	Location	Distance to surface (mm)	Surface area (mm^2)	Volume (mm^3)
1	Spherical	Internal	0.42	1.7E−02	18.9E−05
2	Hemispherical	Surface	0	1.5E−02	14E−05
3	Oblate hemispherical	Surface	0.46	0.3E−02	1.6E−05
			0.46	0.4E−02	2.7E−05
4	Spherical	Internal	0.21	0.6E−02	3.7E−05
5	Hemispherical	Surface	0	1.1E−02	9.8E−05
6	Oblate cuboid	Surface	0.34	1.0E−02	7.7E−05
	Oblate hemispherical		0.44	1.3E−02	12.1E−05

4. Fatigue Life Prediction Methods

4.1. Fatigue crack initiation model considering K_t

Figure. 9 shows the flow chart to a sequence of crack initiation analysis through simulation. As was introduced in the theoretical background, the boundary condition for RVE models was used PBC and subjected to the stress level of 80−200 MPa. *.ODB (output database) file, including stress and strain of RVE models, is generated from ABAQUS through FE analysis.

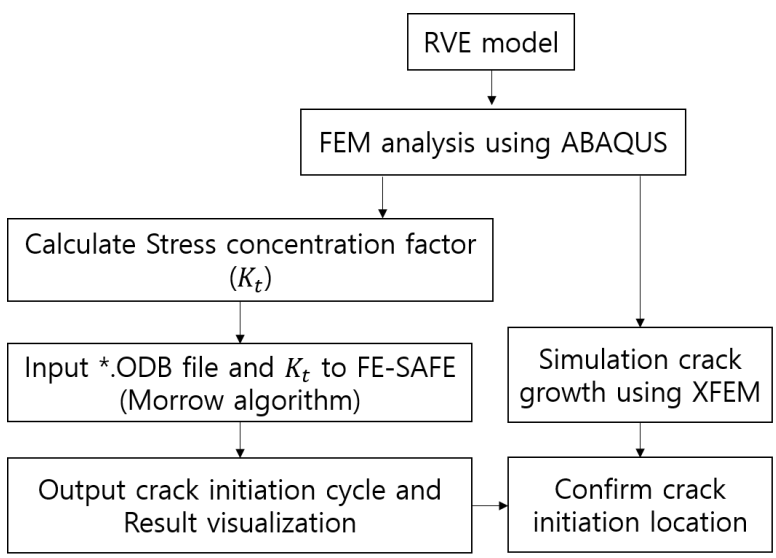

Figure. 9. Flow chart of crack initiation model analysis.

The stress concentration factor (K_t) was obtained by calculation with maximum stress (equivalent Von Mises) and normal stress (Figure. 10). The crack initiation cycle was calculated by inputting *.ODB file and K_t generated on ABAQUS to FE-SAFE. FE-SAFE tool calculated through Morrow algorithm-based strain-life with pre-input material (AlSi10Mg) properties.

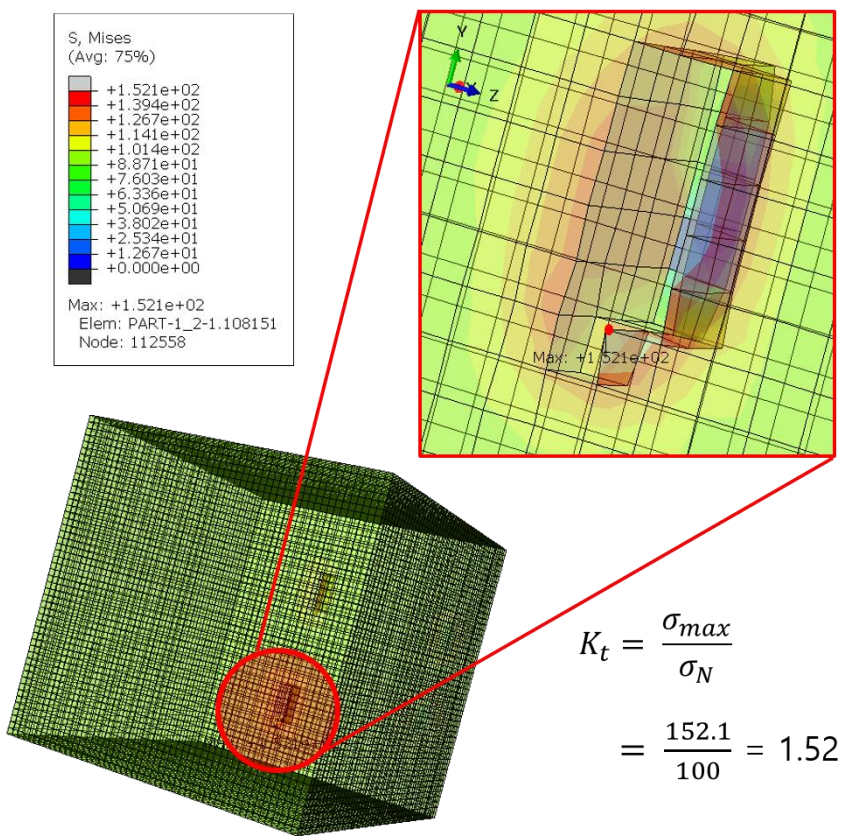

Figure. 10. Stress concentration factor of RVE-3.

For mean stress effect and plastic condition, the Morrow equation, which developed with Coffin-Manson equation, was selected. The material parameters adopted for the Morrow algorithm were value verified through experiments in reference [50]. Morrow equation coefficients used are from Table 4.

Table 4 Morrow equation coefficients

σ'_f	b	ε'_f	c
327.5	−0.074	0.097	−0.564

To have the efficiency of time through minimization of analysis, cycles for other stress levels were calculated in one *.ODB file using the scale factor as an internal function of FE-SAFE for the initial stress. Using results of FE-SAFE, crack initiation location can be found through *.ODB file containing the log life. This crack initiation location was compared with the point found by XFEM (extended finite element method) simulation on ABAQUS and verified (Figure 11.).

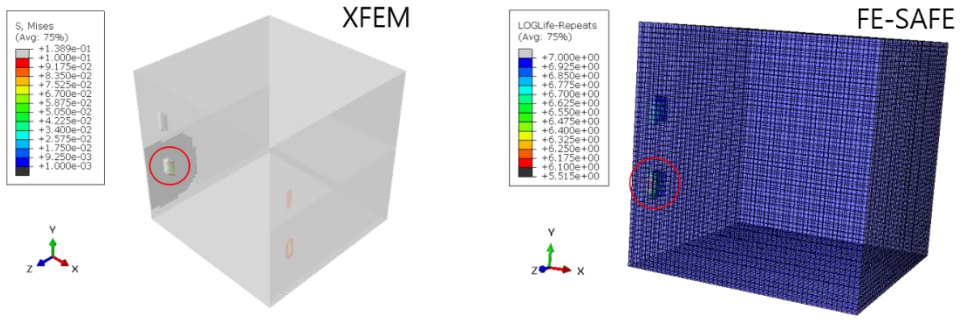

Figure. 11. Crack initiation location comparison of RVE−3

4.2. Fatigue crack growth model

Crack growth model analysis was performed based on Fracture Mechanics. In this thesis, Paris's equation and Murakami concept were adopted.

The reason for adopting Paris's equation was that this equation was sufficient to the crack initiation model and critical value although this was satisfied only in Region II. Besides fracture toughness called critical value (K_c) in Region III also was directly obtained by XFEM simulation and verified with values of other references. Therefore, Paris's equation in Region II was enough to estimate total fatigue life. The mean stress effect was not included in conditions because the model's load ratio to be verified was negative (R = −1), so it was

unnecessary to apply it to crack growth model by the concept of Walker model.

Murakami concept was chosen because it was necessary to find out crack growth by increasing the crack area, not the size to consider pores' effect. Besides, in order to verify the model considering elastic and plastic phase, the analysis using ΔK was limited, so energy release rate G, also called driving force, was used instead. The relationship between G and J−Integral [51] can be shown as Eq. 18, and it was converted into ΔK and applied to the crack growth model (Eq. 19).

$$\mathbf{G} = -\frac{dU}{dA} \quad \mathbf{\Delta J} = \frac{\mathbf{\Delta K^2}}{E'} = \boldsymbol{G} \tag{18}$$

$$\mathbf{\Delta K} = \sqrt{\boldsymbol{E'\,K}} \qquad \frac{\mathbf{da}}{dN} = \mathbf{C}(\sqrt{\boldsymbol{E'\,K}})^{\boldsymbol{m}} \tag{19}$$

Where E'=E is Young's modulus for plane stress condition and $E' = \mathrm{E}/(1-\nu^2)$ is Young's modulus for plane strain condition. Flow chart of crack propagation simulation are illustrated in Figure. 12 developed in [24]

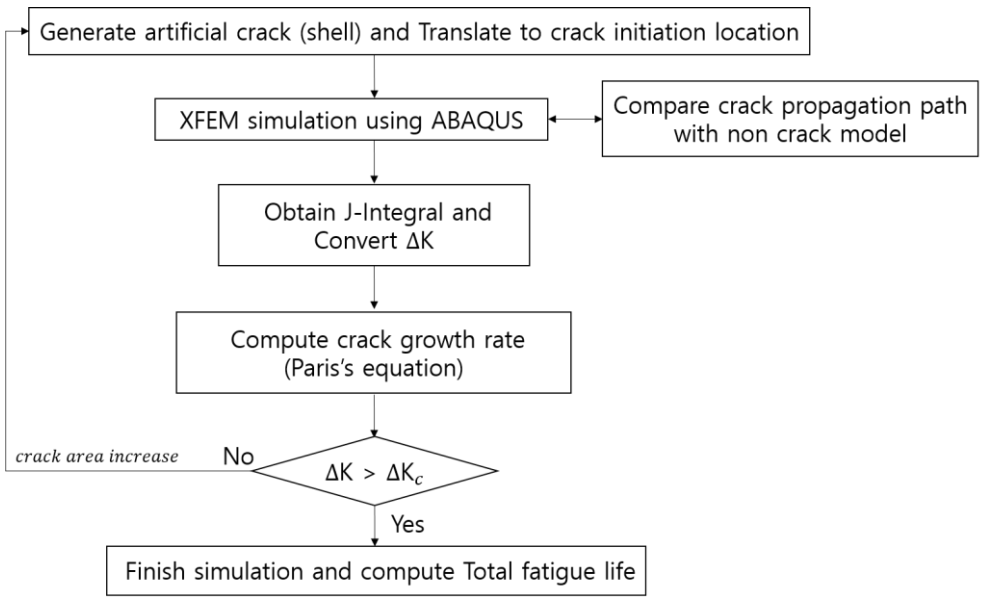

Figure. 12. Flow chart of crack propagation simulation

Using XFEM simulation on ABAQUS, crack initiation location, and growth path were obtained as shown in Figure. 13. A shell-shaped 3D artificial crack was created in that location and analyzed again with XFEM. Regardless of the presence or absence of artificial cracks, this crack was moved by comparing each crack growth path and adjusting the exact crack location. After determining the artificial crack location, it increased the artificial crack area by following the crack path of each step of the XFEM simulation. J-integral and SIF were calculated by increasing the crack area and inputted into the

crack growth model. When SIF increase rapidly or fluctuates broadly, the SIF at that time was defined as Critical value (K_c). The crack propagation cycle was calculated by numerical integrating the crack propagation up to this area, and simulation was terminated.

The equation for obtaining the crack propagation cycle through numerical integration is as follows.

$$N_p = \frac{1}{C}\int_{\sqrt{area_i}}^{\sqrt{area_f}} \frac{1}{\Delta K^m} d\left(\sqrt{area}\right) \quad (20)$$

Where $area_i$ and $area_f$ mean artificial crack area at crack initiation and at the moment of failure, respectively. When the simulation was finished, total fatigue life was obtained by adding crack initiation cycle (N_i) by numerical integrating and crack propagation cycle (N_p) obtained by FE-SAFE.

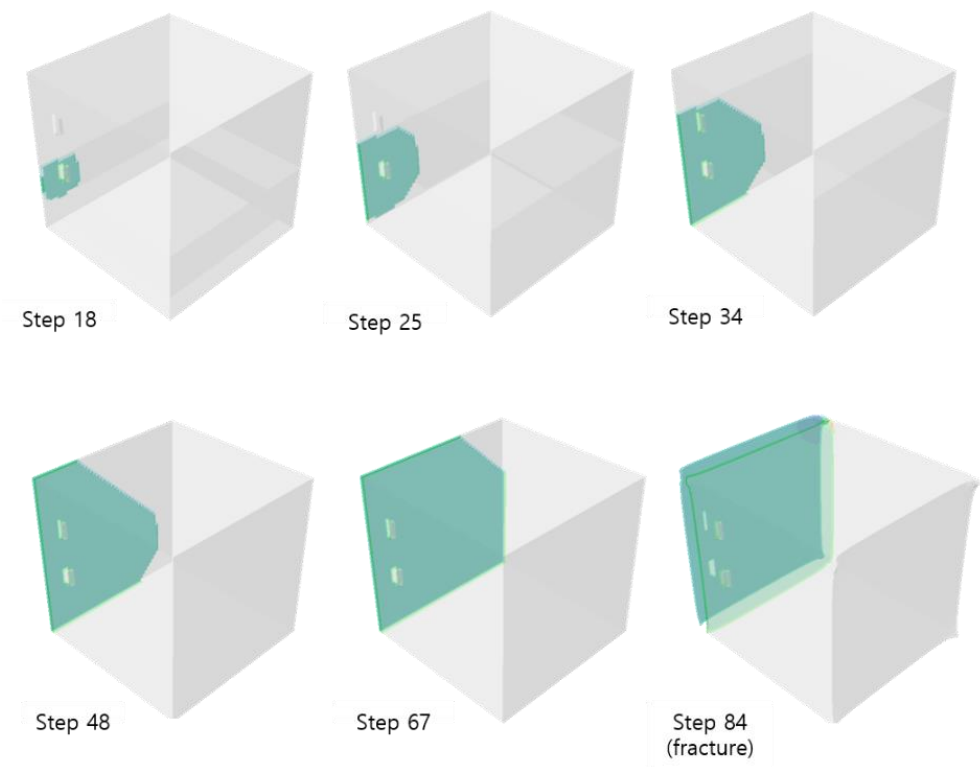

Figure. 13. Crack propagation path of RVE−3

5. Result and Discussion

5.1. Simulation result of crack initiation model

RVE models generated from CT images were analyzed through simulation with the elastic−plastic 3D FE model under uniaxial cyclic loading. Stress concentration factor (K_t) calculated using FE model analysis had different values according to RVE model with different pore geometries and location, respectively. These K_t values were influenced by volume and shape of the pore and the correlation was examined through the information of the pore and value of K_t. Besides, it has been presented in the reference [39,40] that the model of larger K_t value tend to be the shorter the life. Comparison with $K_t=1$ (which does not reflect the effect of pores) through simulation resulted as shown in Figure. 14.

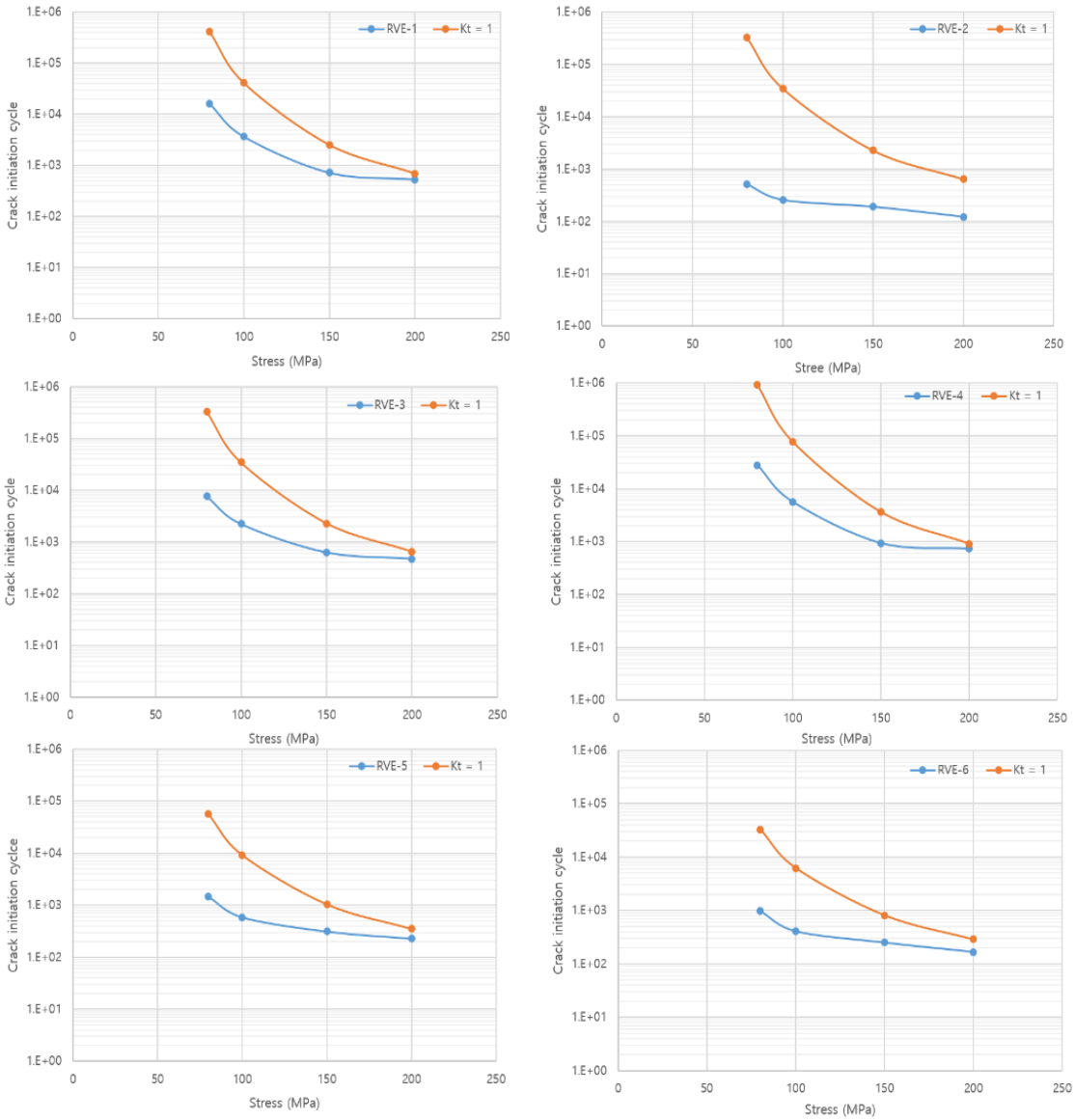

Figure. 14. N_i of RVE models

The pore's information was referenced in Table 3 to determine the priority of the factors that affect each RVE models' pores.

Values of K_t were obtained, as shown in the Figure. 14−15 using the results of FE model analysis were performed through ABAQUS. It represents the value calculated by applying maximum stress of 100 MPa (Figure. 15−16). The pores had a constant K_t value up to certain stress (100 MPa) and K_t value had been shown to decrease with values more than that stress. It means that the degree to which the stress was concentrated in the pores decreases due to the occurrence of plastic deformation of the ductile material, in the vicinity of the pores. Values of K_t for each stress are shown in Table 5.

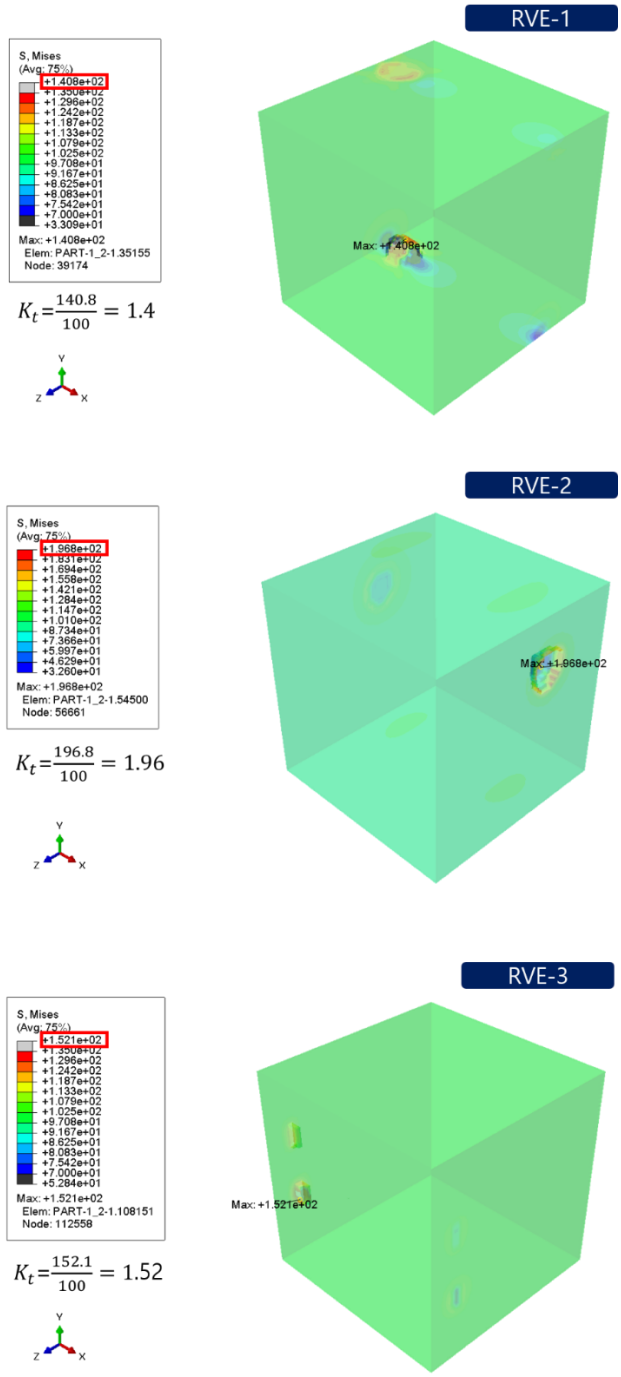

Figure. 15. K_t of RVE models (1−3) at stress level of 100 MPa

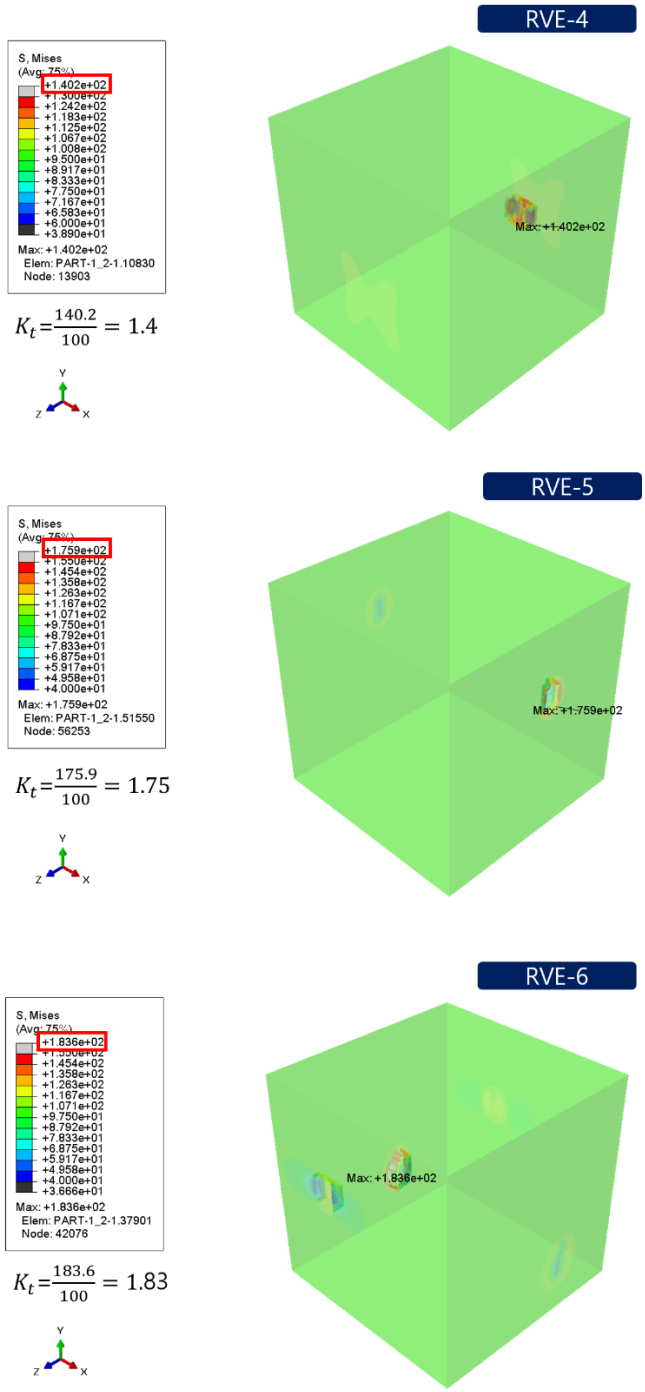

Figure. 16. K_t of RVE models (4−6) at stress level of 100 MPa

Table 5 K_t of each RVE models for each stress

RVE	Stress Concentration factor			
	80 MPa	100 MPa	150 MPa	200 MPa
1	1.408	1.408	1.341	1.089
2	1.967	1.968	1.441	1.235
3	1.521	1.521	1.364	1.106
4	1.401	1.402	1.345	1.107
5	1.758	1.759	1.404	1.169
6	1.836	1.836	1.420	1.207

Values of K_t obtained for each model and *.ODB file of simulation by ABAQUS was used to obtain data, as shown in Table 6-8. Through this process, the crack initiation cycle and location were obtained, and the visualization of this result expresses the life contour and worst life, as shown in Figure. 17. This visualized result is expressed on the log scale, and the worst life means that life have the lowest lifetime point in this result. The point is regarded as the location where the crack is generated. It can be compared that this is the same location as the crack initiation location in XFEM simulation.

Table 6 Result of FE-SAFE siumulation applied 80MPa

RVE	Crack initiation cycle	
	Log life	Actual life(cycle)
1	4.199	15826
2	2.738	547
3	3.882	7617
4	4.445	27848
5	3.160	1447
6	2.972	937

Table 7 Result of FE-SAFE siumulation applied 100MPa

RVE	Crack initiation	
	Log life	Actual life(cycle)
1	3.562	3649
2	2.408	256
3	3.348	2226
4	3.750	5619
5	2.767	585
6	2.611	408

Table 8 Result of FE-SAFE siumulation applied 200MPa

RVE	Crack initiation cycle	
	Log life	Actual life(cycle)
1	2.728	534
2	2.089	122
3	2.673	471
4	2.864	731
5	2.358	228
6	2.223	167

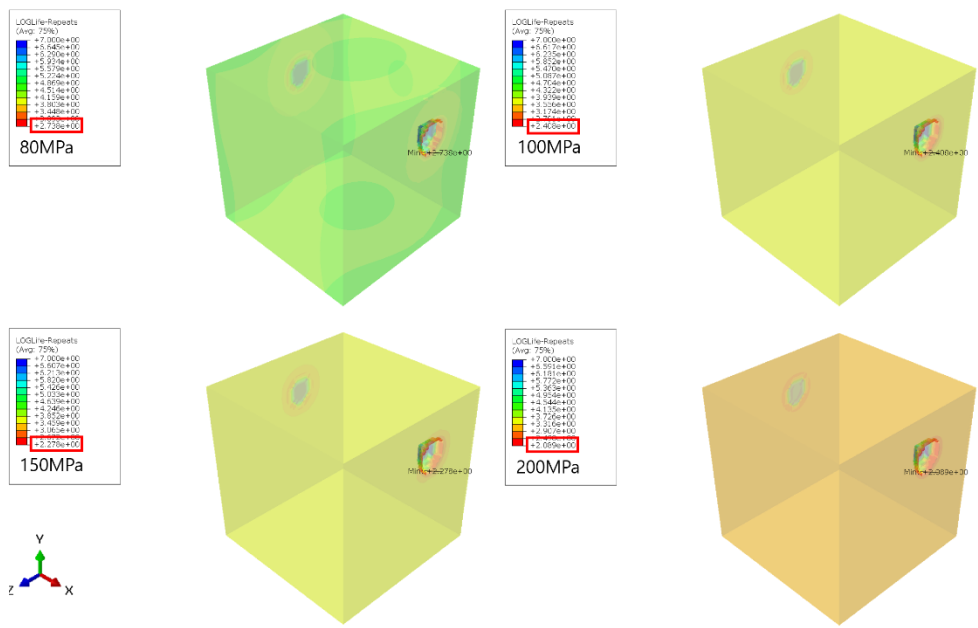

Figure. 17. Log-life of RVE-2

Through the analysis of the crack initiation model, it was possible to prioritize the factors affecting K_t for the volume, shape, and the number of pores. As a result of FE analysis, it was shown that K_t was most affected by pore's volume. The model with the highest K_t was RVE−2 model, which is a relatively bulky model with a hemispherical shape. Conversely, the model with a spherical shape with closed all directions showed a low K_t. In other words, the crack initiation cycle of the model with a pore with large volume has shorter than that of other models. Except for the pore's volume, it was found through the comparison of RVE−3 model and RVE−4 that the number of the pore also affect the crack initiation cycle.

5.2. Simulation result of crack propagation model

5.2.1. Fatigue crack growth rate

It was calculated SIF to be applied to the crack growth model to obtain the crack propagation cycle. Since the model to be verified includes a plastic phase, J−integral was used. This value was continuously obtained by increasing the crack area using python code to get the final fracture area, and this value was changed to SIF through Eq. 18 to apply to the Paris equation. As shown in the result of J−Integral, it can be seen that the value of J increase as the area increases, and the final fracture area decreases as the stress increases.

Rapidly increasing or changing the value of J was used to consider as a critical value through calculating SIF. The area at this time was regarded as the final fracture area ($area_f$). The larger the stress, the smaller the area, and the critical value of simulation results was calculated similarly to the reference value. In Table 9, the critical values for each stress and $\sqrt{area_f}$ are expressed. The crack growth rate was calculated as shown in Figure. 18.

Table 9 $\sqrt{area_f}$ and critical value (K_c) for each stress

RVE	$\sqrt{area_f}$ (mm)			K_c
	80MPa	100MPa	200MPa	
1	0.468	0.459	0.355	39
2	0.432	0.420	0.349	45
3	0.441	0.435	0.380	42
4	0.449	0.419	0.352	41
5	0.439	0.425	0.345	43
6	0.440	0.420	0.337	43

Critical value calculated in the simulation was compared with experimental results. The shape of the specimen and test conditions were different for each experiment. This work particularly simulated a small size of RVE models. However, the critical value is a material-dependent material property and depends only on temperature and loading speed [52]. So, it was compared with the results considering these conditions. As a result, critical values of simulation results showed relatively similar to the experimental results. They are compared through Table 10.

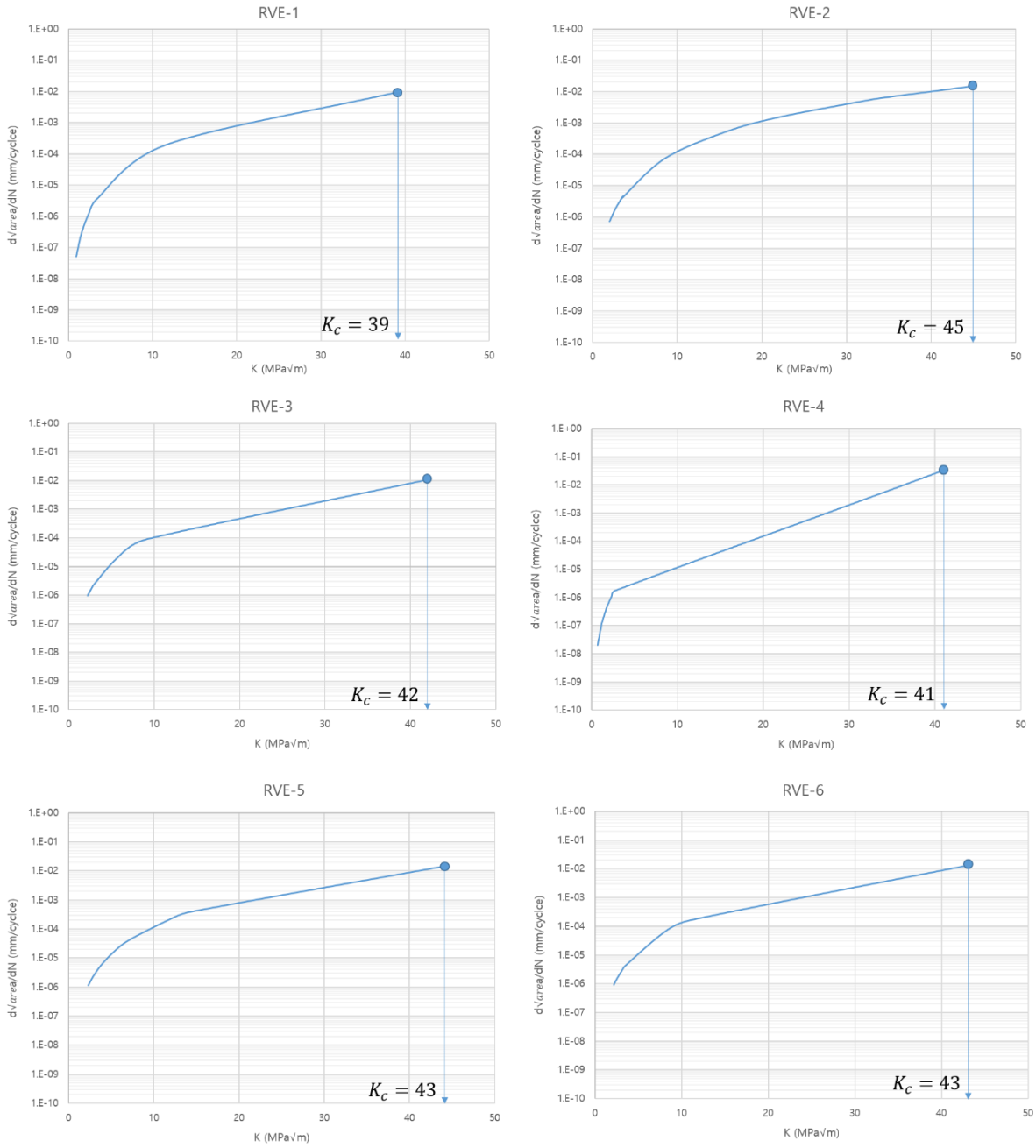

Figure. 18. Fatigue crack growth rate

Table 10 Comparison K_c between reference and simulation

Condition	This work	Hitzler[53]	Suryawanshi[54]
SLM-AlSi10Mg	**39-45** $(MPa\sqrt{m})$	40-60 $(MPa\sqrt{m})$	37-46 $(MPa\sqrt{m})$

5.2.2. Computational result of N_p

Using SIF values and the area where the final fracture occurs obtained in 4.2.1, the crack propagation cycle was calculated by Eq. 20. Similar to the crack initiation cycle's tendency, it can be seen that the cycle of the model with pore with large volume showed a larger value than the other models. The crack propagation cycle for each model can be seen in Table 11.

Table 11 Crack propagation cycle for each stress

RVE	Crack propagation cycle		
	80MPa	100MPa	200MPa
1	2.E+06	1.E+06	2.E+04
2	3.E+05	1.E+05	5.E+03
3	5.E+05	3.E+05	1.E+04
4	8.E+06	4.E+06	1.E+05
5	4.E+05	1.E+05	7.E+03
6	3.E+05	1.E+05	3.E+03

5.3. Estimate of Total fatigue life

5.3.1. Total fatigue life (N_f)

The total fatigue life (N_f) of RVE models were calculated as the sum of crack initiation cycle (N_i) and the propagation cycle (N_p). In other words, the cycle from the generation of crack to final fracture was calculated. To compare the proportion of crack initiation and crack propagation in total fatigue life, the cycle calculated for the RVE−1 model is represent, as shown in Figure. 19.

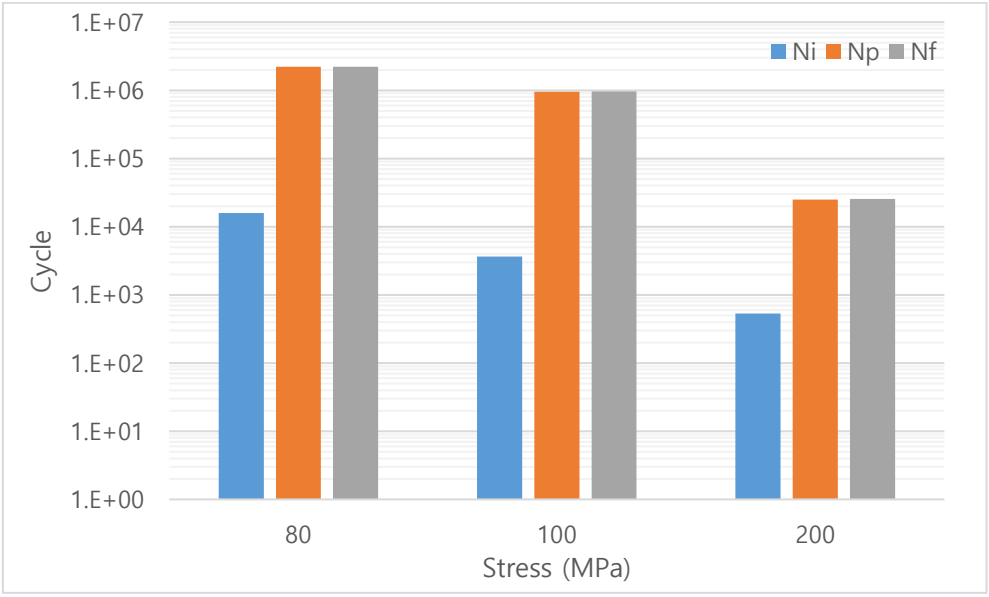

Figure. 19. Total fatigue life of RVE−1

It can be seen that the crack initiation cycle had a low proportion of the total fatigue life for the RVE-1 model as well as the other RVE models with pores. This can also be seen at stress concentration such as notch and crack initiation cycle is short when the crack is generated from defects such as pores as in this RVE model. This can be known from reference [52]. For this reason, some researchers [55] neglect the crack initiation phase when analyzing the fatigue life of structures with defects.

The proportion of crack propagation reduces as the stress increase. Because of the larger the stress, the greater the rate of reduction in the crack propagation cycle than the crack initiation cycle is shown. The effect of each model's pore on the total fatigue life can be analyzed through Figure. 2. Through this result, it can be seen that the volume of the pore is greatly affected. RVE models with small pores had a longer life than models with bulky pores.

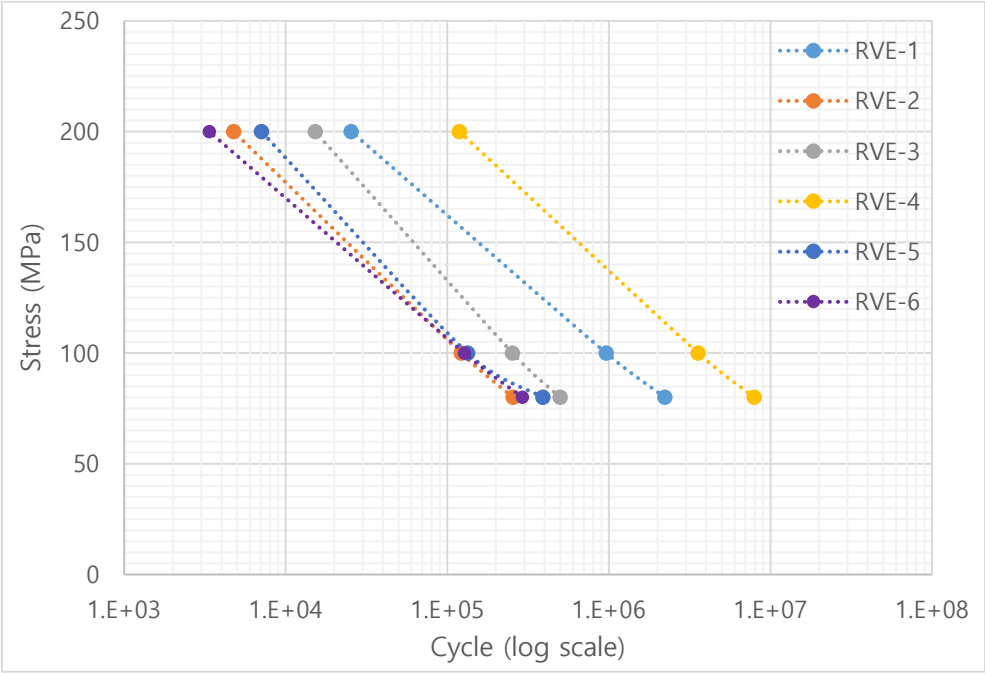

Figure. 20. S-N curve of RVE models

5.3.2. Validation of N_f with simulation results

Experimental results validated these simulation results. The total fatigue life was calculated for 10 RVE models, including RVE-1~6, and compared with the experimental results [55-59] for the fatigue life of AM AlSi10Mg by SLM. Figure. 21 shows that total fatigue life agrees to some extent at low-stress level, although some differences occurred at a high stress level.

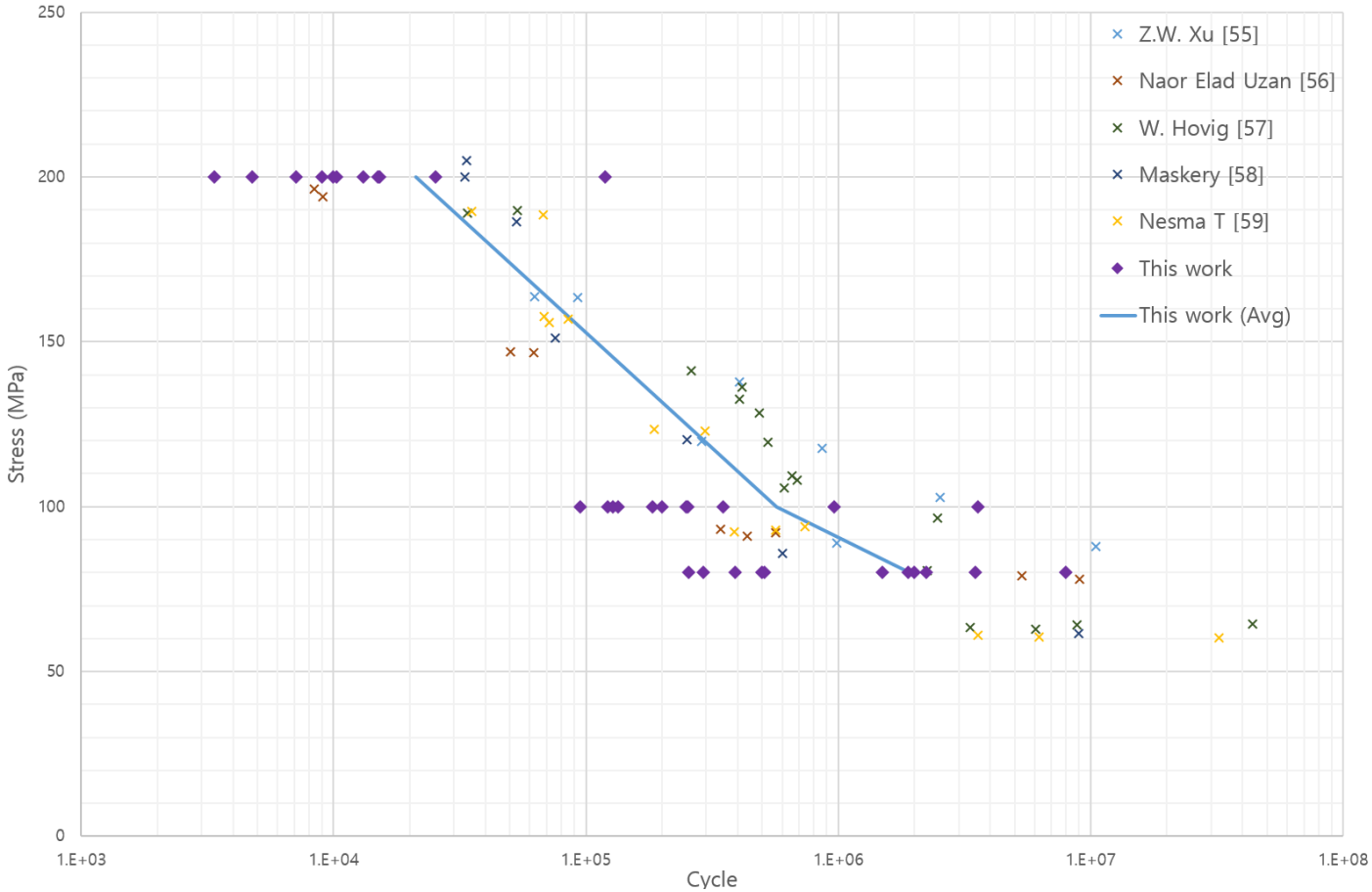

Figure. 21. Comparison N_f between reference and simulation

5.3.3. The effect of pores on fatigue life

Estimating the effect of pores on total fatigue life, pore's volume appeared to be the most important factor. Although the effect on the location of pores could not be evaluated by imposing PBC, it was confirmed that the model with the bulky pores showed a short fatigue life. Besides, the shape and number of pores excluding the volume influenced the fatigue life through each model.

The effect of pores can be estimated for the divided phases of fatigue life through simulation. The entire life of individual RVE models was not significantly different depending on the pore's volume and shape for each stress. With the results of total fatigue life compared with various experimental data, pore's tendency to affect fatigue life was confirmed.

6. Conclusion and future works

6.1. Conclusion

The strain-life method and Fracture Mechanical approach proposed in this thesis includes a finite element (FE) based simulation to calculate the total fatigue life of Additive manufacturing AlSi10Mg by SLM. CT image was subjected to image processing to generate a 3D FE model, and several RVEs were randomly made through MATLAB code for FE analysis. By comparing the simulation results with the total fatigue life of reference dealing with the test results of AlSi10Mg in similar conditions, it is found that cycle is reasonably agreed.

The total fatigue life is divided into two stages to estimate pores' effect and these effects of pores at each stage are similar. In the fatigue life cycle of materials with defects such as pores, the crack initiation cycle is small, and the proportion of the crack propagation cycle is large as in other experiments. Considering the influence of pores, critical factor of pores is the volume. Many factors influence fatigue life, such as the shape and number of pores, but the

volume is the factor affected the most is. The difference between fatigue life of model with bulky pores and model with small pores is the greatest. The larger stress, the smaller fracture area where the final fracture occurred for each stress in the crack propagation simulation. It is also verified that the area where this fracture occurs is proportional to the size of the initial pore.

Although the simulation and experimental values did not match perfectly, this was caused by the difference in SLM process parameters, porosity and loading condition, etc. However, the fatigue life of AM materials by the SLM process could be predicted, and pore's effect could be evaluated.

6.2. Future works

To estimate fatigue life, the RVE approach is used to evaluate pore's effect and fatigue life. However, when generating the RVE, the model had a limitation with lower porosity. Since the models with no pores were sometimes created, many RVE models need to be generated, and values of them must be analyzed and evaluated, although there were no models without pores in this study.

When increasing the crack area to calculate the crack propagation cycle, there were strange models of the shape where it was difficult to increase the crack area to fit the crack propagation path by XFEM. Although the artificial crack was increased somewhat consistently for the model, increasing to the irregularly shaped crack area, this limitation should be improved for accurate fatigue life estimate.

Reference

[1] S. Lee *et al.*, “Wohleres Report 2014,” 2012.

[2] D. D. Gu, W. Meiners, K. Wissenbach, and R. Poprawe, ""Laser additive manufacturing of metallic components: Materials, processes and mechanisms,"" *Int. Mater. Rev.*, vol. 57, no. 3, pp. 133–164, May 2012.

[3] ISO/ASTM, ""Additive Manufacturing – General Principles Terminology (ASTM52900),"" *Rapid Manuf. Assoc.*, pp. 10–12, 2013.

[4] W. E. Frazier, ""Metal additive manufacturing: A review,"" *J. Mater. Eng. Perform.*, vol. 23, no. 6, pp. 1917–1928, 2014.

[5] M. Javaid and A. Haleem, ""Additive manufacturing applications in medical cases: A literature based review,"" *Alexandria J. Med.*, vol. 54, no. 4, pp. 411–422, 2018.

[6] G. Bansal, D. Bandhu Singh, H. Singh Virk, A. Devrani, and A. Bhandari, ""Microstructural characterization, applications and process study of various additive manufacturing process: A review,"" *Mater. Today Proc.*, pp. 1–5, 2020.

[7] E. O. Olakanmi, R. F. Cochrane, and K. W. Dalgarno, ""A review on selective laser sintering/melting (SLS/SLM) of aluminium alloy powders: Processing, microstructure, and properties,"" *Prog. Mater. Sci.*, vol. 74, pp. 401–477, 2015.

[8] S. Tammas-Williams, P. J. Withers, I. Todd, and P. B. Prangnell, ""The Influence of Porosity on Fatigue Crack Initiation in Additively Manufactured Titanium Components,"" *Sci. Rep.*, vol. 7, no. 1, pp. 1–13, 2017.

[9] N. Sanaei, A. Fatemi, and N. Phan, ""Defect characteristics and analysis of their variability in metal L-PBF additive manufacturing,"" *Mater. Des.*, vol. 182, p. 108091, 2019.

[10] B. Zhang, Y. Li, and Q. Bai, ""Defect Formation Mechanisms in Selective Laser Melting: A Review,"" *Chinese J. Mech. Eng. (English*

Ed., vol. 30, no. 3, pp. 515–527, May 2017.

[11] H. Gong, K. Rafi, H. Gu, T. Starr, and B. Stucker, ""Analysis of defect generation in Ti–6Al–4V parts made using powder bed fusion additive manufacturing processes,"" *Addit. Manuf.*, vol. 1, pp. 87–98, 2014.

[12] A. Fatemi, R. Molaei, S. Sharifimehr, N. Phan, and N. Shamsaei, ""Multiaxial fatigue behavior of wrought and additive manufactured Ti–6Al–4V including surface finish effect,"" *Int. J. Fatigue*, vol. 100, pp. 347–366, 2017.

[13] S. Leuders, S. Meiners, L. Wu, A. Taube, T. Tröster, and T. Niendorf, ""Structural components manufactured by Selective Laser Melting and Investment Casting—Impact of the process route on the damage mechanism under cyclic loading,"" *J. Mater. Process. Technol.*, vol. 248, no. May, pp. 130–142, 2017.

[14] S. Tammas–Williams, P. J. Withers, I. Todd, and P. B. Prangnell, ""Porosity regrowth during heat treatment of hot isostatically pressed additively manufactured titanium components,"" *Scr. Mater.*, vol. 122, pp. 72–76, 2016.

[15] V. D. Le, E. Pessard, F. Morel, and F. Edy, ""Influence of porosity on the fatigue behaviour of additively fabricated TA6V alloys,"" in *MATEC Web of Conferences*, May 2018, vol. 165.

[16] E. Brandl, U. Heckenberger, V. Holzinger, and D. Buchbinder, ""Additive manufactured AlSi10Mg samples using Selective Laser Melting (SLM): Microstructure, high cycle fatigue, and fracture behavior,"" *Mater. Des.*, vol. 34, pp. 159–169, 2012.

[17] E. Santecchia *et al.*, ""A Review on Fatigue Life Prediction Methods for Metals,"" *Adv. Mater. Sci. Eng.*, vol. 2016, 2016.

[18] A. M. P. De Jesus, A. L. L. Da Silva, and J. A. F. O. Correia, ""Fatigue of riveted and bolted joints made of puddle iron – A numerical approach,"" *J. Constr. Steel Res.*, vol. 102, pp. 164–177, 2014.

[19] M. Mlikota, S. Schmauder, and Božić, ""Calculation of the Wöhler (S–N) curve using a two–scale model,"" *Int. J. Fatigue*, vol. 114, no. December 2017, pp. 289–297, 2018.

[20] Y. Murakami and H. Usuki, ""Quantitative evaluation of effects of non-metallic inclusions on fatigue strength of high strength steels. II: Fatigue limit evaluation based on statistics for extreme values of inclusion size,"" 1989.

[21] J. C. Newman, ""A CRACK OPENING STRESS EQUATION FOR FATIGUE CRACK GROWTH,"" *Thought A Rev. Cult. Idea*, vol. 24, pp. 131–135, 1984.

[22] M. S. Forman RG, ""A study of the microstructural evolution during selective laser melting of Ti–6Al–4V,"" *Fracture Mechanics: 22nd Symposium, Vol. 1*, 1992.

[23] M. Tang and P. C. Pistorius, ""Fatigue life prediction for AlSi10Mg components produced by selective laser melting,"" *Int. J. Fatigue*, vol. 125, no. April, pp. 479–490, 2019.

[24] R. Hidalgo, J. A. Esnaola, I. Llavori, M. Larrañaga, I. Hurtado, and N. Herrero-Dorca, ""Fatigue life estimation of cast aluminium alloys considering the effect of porosity on initiation and propagation phases,"" *Int. J. Fatigue*, vol. 125, no. January, pp. 468–478, 2019.

[25] S. Romano, S. Miccoli, and S. Beretta, ""A new FE post-processor for probabilistic fatigue assessment in the presence of defects and its application to AM parts,"" *Int. J. Fatigue*, vol. 125, no. April, pp. 324–341, 2019.

[26] P. Grohs, ""Estimation of the Fatigue Life of Additively Manufactured Metallic Components Using Modified Strain Life Parameters Based on Surface Roughness,"" 2019.

[27] E. Wycisk, A. Solbach, S. Siddique, D. Herzog, F. Walther, and C. Emmelmann, ""Effects of defects in laser additive manufactured Ti-6Al-4V on fatigue properties,"" *Phys. Procedia*, vol. 56, no. C, pp. 371–378, 2014.

[28] S. Leuders, M. Vollmer, F. Brenne, T. Tröster, and T. Niendorf, ""Fatigue Strength Prediction for Titanium Alloy TiAl6V4 Manufactured by Selective Laser Melting,"" *Metall. Mater. Trans. A Phys. Metall. Mater. Sci.*, vol. 46, no. 9, pp. 3816–3823, 2015.

[29] S. Siddique *et al.*, ""Computed tomography for characterization of fatigue performance of selective laser melted parts,"" *Mater. Des.*,

vol. 83, pp. 661–669, 2015.

[30] T. Kanit, S. Forest, I. Galliet, V. Mounoury, and D. Jeulin, ""Determination of the size of the representative volume element for random composites: Statistical and numerical approach,"" *Int. J. Solids Struct.*, vol. 40, no. 13–14, pp. 3647–3679, 2003.

[31] F. R. Liu, K. C. Chan, and C. Y. Tang, ""Numerical modeling of the thermo-mechanical behavior of particle reinforced metal matrix composites in laser forming by using a multi-particle cell model,"" *Compos. Sci. Technol.*, vol. 68, no. 9, pp. 1943–1953, 2008.

[32] Q. Zhang, Z. Zuo, and J. Liu, ""Numerical analysis for the influence of casting micro porosity on fatigue life,"" *Eng. Fail. Anal.*, vol. 48, pp. 11–20, 2015.

[33] J. Yu, C. Zhou, and H. Zhang, ""A micro-image based reconstructed finite element model of needle-punched C/C composite,"" *Compos. Sci. Technol.*, vol. 153, pp. 48–61, 2017.

[34] W. Wu, J. Owino, A. Al-Ostaz, and L. Cai, ""Applying Periodic Boundary Conditions in Finite Element Analysis,"" *2014 SIMULIA Community Conf.*, no. Figure 1, pp. 1–13, [Online]. Available:

[35] S. M. Beden, S. Abdullah, and A. K. Ariffin, *Review of fatigue crack propagation models for metallic components*, vol. 28, no. 3. 2009.

[36] R. A. Hardin and C. Beckermann, ""Prediction of the fatigue life of cast steel containing shrinkage porosity,"" *Metall. Mater. Trans. A Phys. Metall. Mater. Sci.*, vol. 40, no. 3, pp. 581–597, 2009.

[37] F. Kun, H. A. Carmona, J. S. Andrade, and H. J. Herrmann, ""Universality behind Basquin' 's law of fatigue,"" *Phys. Rev. Lett.*, vol. 100, no. 9, 2008.

[38] M. Ghodrati and R. Mirzaeifar, ""Computational Study of Fatigue in Sub-grain Microstructure of Additively Manufactured Alloys,"" *J. Mater. Eng. Perform.*, vol. 29, no. 7, pp. 4631–4640, 2020.

[39] G. Qian, Z. Jian, Y. Qian, X. Pan, X. Ma, and Y. Hong, ""Very-high-cycle fatigue behavior of AlSi10Mg manufactured by selective laser melting: Effect of build orientation and mean stress,"" *Int. J. Fatigue*, vol. 138, no. May, p. 105696, 2020.

[40] S. Hassanifard and S. M. Hashemi, ""On the strain–life fatigue parameters of additive manufactured plastic materials through fused filament fabrication process,"" *Addit. Manuf.*, vol. 32, no. September 2019, p. 100973, 2020.

[41] A. Ince and G. Glinka, ""A modification of Morrow and Smith–Watson–Topper mean stress correction models,"" *Fatigue Fract. Eng. Mater. Struct.*, vol. 34, no. 11, pp. 854–867, 2011.

[42] J. Wang *et al.*, ""Influence of surface porosity on fatigue life of additively manufactured ASTM A131 EH36 steel,"" *Int. J. Fatigue*, vol. 142, no. April 2020, p. 105894, 2021.

[43] R. Biswal, A. K. Syed, and X. Zhang, ""Assessment of the effect of isolated porosity defects on the fatigue performance of additive manufactured titanium alloy,"" *Addit. Manuf.*, vol. 23, no. July, pp. 433–442, 2018.

[44] P. Paris and F. Erdogan, ""A critical analysis of crack propagation laws,"" *J. Fluids Eng. Trans. ASME*, vol. 85, no. 4, pp. 528–533, 1963.

[45] N. H. Dao and H. Sellami, ""Stress intensity factors and fatigue growth of a surface crack in a drill pipe during rotary drilling operation,"" *Eng. Fract. Mech.*, vol. 96, pp. 626–640, 2012.

[46] Y. N. Hu *et al.*, ""A new approach to correlate the defect population with the fatigue life of selective laser melted Ti–6Al–4V alloy,"" *Int. J. Fatigue*, vol. 136, no. March, 2020.

[47] Y. Murakami, *Metal Fatigue: Effects of Small Defects and Nonmetallic Inclusions*. 2002.

[48] A. Parts, B. J. Mfusi, N. R. Mathe, and L. C. Tshabalala, ""The Effect of Stress Relief on the Mechanical and Fatigue Properties of Additively Manufactured AlSi10Mg Parts,"" *Metals (Basel).*, vol. 9, p. 1216, 2019.

[49] S. Sarkar, C. S. Kumar, and A. K. Nath, ""Effects of heat treatment and build orientations on the fatigue life of selective laser melted 15–5 PH stainless steel,"" *Mater. Sci. Eng. A*, vol. 755, no. March, pp. 235–245, 2019.

[50] S. Romano, L. Patriarca, S. Foletti, and S. Beretta, ""LCF behaviour and a comprehensive life prediction model for AlSi10Mg obtained by SLM,"" *Int. J. Fatigue*, vol. 117, no. July, pp. 47–62, 2018.

[51] J. R. Rice, ""A path independent integral and the approximate analysis of strain concentration by notches and cracks,"" *J. Appl. Mech. Trans. ASME*, vol. 35, no. 2, pp. 379–388, 1964.

[52] M. Richard, HA & Sander, *Fatigue crack growth : detect–assess–avoid*, no. 1st ed. Cham, Switzerland : Springer, 2016.

[53] L. Hitzler *et al.*, ""Fracture toughness of selective laser melted AlSi10Mg,"" *Proc. Inst. Mech. Eng. Part L J. Mater. Des. Appl.*, vol. 233, no. 4, pp. 615–621, 2019.

[54] J. Suryawanshi, K. G. Prashanth, S. Scudino, J. Eckert, O. Prakash, and U. Ramamurty, ""Simultaneous enhancements of strength and toughness in an Al–12Si alloy synthesized using selective laser melting,"" *Acta Mater.*, vol. 115, pp. 285–294, 2016.

[55] Z. W. Xu, Q. Wang, X. S. Wang, C. H. Tan, M. H. Guo, and P. B. Gao, ""High cycle fatigue performance of AlSi10mg alloy produced by selective laser melting,"" *Mech. Mater.*, vol. 148, no. June, 2020.

[56] N. E. Uzan, R. Shneck, O. Yeheskel, and N. Frage, ""Fatigue of AlSi10Mg specimens fabricated by additive manufacturing selective laser melting (AM–SLM),"" *Mater. Sci. Eng. A*, vol. 704, no. February, pp. 229–237, 2017.

[57] E. W. Hovig, A. S. Azar, M. F. Sunding, E. Andreassen, and K. Sørby, ""High cycle fatigue life estimation of materials processed by laser powder bed fusion,"" *Fatigue Fract. Eng. Mater. Struct.*, vol. 42, no. 7, pp. 1454–1466, 2019.

[58] I. Maskery *et al.*, ""Fatigue performance enhancement of selectively laser melted aluminium alloy by heat treatment,"" *Proc. – 26th Annu. Int. Solid Free. Fabr. Symp. – An Addit. Manuf. Conf. SFF 2015*, no. 2015, pp. 1017–1025, 2020.

[59] N. T. Aboulkhair, ""mechanical properties . PhD thesis , University of Additive manufacture of an aluminium alloy : processing , microstructure , and,"" no. December, 2016.

국문초록

변형률-수명 방법과 파괴역학 접근에 의한 적층제조된 AlSi10Mg의 피로수명 평가

송 윤 선
항공우주공학과
서울대학교 대학원

3D 프린팅 기술 / 적층제조 에서 널리 알려져 있는 선택적 레이저 용융방식으로 제조된 합금은 기존의 공정방식에 비해 설계의 유연성과 생산 효율성의 장점을 가진다. 특히 적층제조로 공정된 티타늄과 알루미늄 합금은 항공 및 의료분야에서 많이 이용된다. 하지만 이 공정과정에서 합금에 생기는 기공과 같은 내부적 결함을 제거하기 위해 열처리 과정을 진행하나 완벽한 제거는 불가피하다. 따라서 적층제조의 합금의 피로수명은 기공의 영향을 고려해서 평가되어야 한다. 본 논문에서 적층제조 방식으로 공정된 알루미늄 합금의 단층촬영(CT) 이미지로 기공이 포함된 대표체적요소(RVE)를 만들어 이에 대해 피로수명을 해석하였다. 피로수명 해석을 위해 균열 시작주기는

변형률-수명 방법을, 균열 성장주기는 파괴역학 접근을 적용하였다. RVE는 CT 이미지를 이미지 처리 알고리즘을 통해 이미지의 품질을 증가시키고, 기공의 입자를 분리시켜 만들었다. 통계적 해석을 위해 다수의 RVE에 주기적 경계조건을 적용하여 3차원 유한요소 해석을 통해 응력과 변형률을 구했다. 유한요소 해석과 피로수명 해석에 필요한 값들을 상용 소프트웨어인 ABAQUS 와 FE-SAFE를 이용하였고, Python 과 MATLAB을 통해 후처리 및 수치 적분으로 총 피로수명을 계산하였다. RVE의 기공 정보와 피로수명의 관계를 분석한 결과 기공의 부피에 가장 큰 영향을 받았으며, 문헌의 실험 결과값과 비교하여 다수의 RVE의 피로수명 값과 어느 정도 비슷한 범위를 가지는 것을 확인할 수 있었다.

Keywords : **적층제조, 피로수명, 파괴역학, 균열개시 및 성장, 변형률-수명 방법**

Student Number : 2019-28564